

PAPER

# Possible quantum-spin-liquid state in van der Waals cluster magnet $\text{Nb}_3\text{Cl}_8$





To cite this article: Bo Liu *et al* 2024 *J. Phys.: Condens. Matter* **36** 155602

View the [article online](#) for updates and enhancements.

## You may also like

- [Smooth, homogeneous, high-purity  \$\text{Nb}\_3\text{Sn}\$  superconducting RF resonant cavity by seed-free electrochemical synthesis](#)  
Zeming Sun, Zhaslan Baraissov, Ryan D Porter et al.
- [A review and prospects for  \$\text{Nb}\_3\text{Sn}\$  superconductor development](#)  
Xingchen Xu
- [Analysis of the strain dependence of the superconducting critical properties of single-crystal and polycrystalline  \$\text{Nb}\_3\text{Sn}\$](#)   
He Ding and Yuanwen Gao

# Possible quantum-spin-liquid state in van der Waals cluster magnet $\text{Nb}_3\text{Cl}_8$

Bo Liu<sup>1,2,6</sup>, Yongchao Zhang<sup>1,2,6</sup>, Xin Han<sup>1,2,6</sup>, Jianping Sun<sup>1</sup> , Honglin Zhou<sup>1,2</sup>,  
Chunhong Li<sup>1</sup>, Jinguang Cheng<sup>1,2</sup> , Shaohua Yan<sup>3,4</sup>, Hechang Lei<sup>3,4,\*</sup> , Youguo Shi<sup>1,2,5,\*</sup>,  
Huaixin Yang<sup>1,2,5,\*</sup> and Shiliang Li<sup>1,2,5,\*</sup> 

<sup>1</sup> Beijing National Laboratory for Condensed Matter Physics, Institute of Physics, Chinese Academy of Sciences, Beijing 100190, People's Republic of China

<sup>2</sup> School of Physical Sciences, University of Chinese Academy of Sciences, Beijing 100190, People's Republic of China

<sup>3</sup> Department of Physics and Beijing Key Laboratory of Opto-electronic Functional Materials & Micro-nano Devices, Renmin University of China, Beijing 100872, People's Republic of China

<sup>4</sup> Key Laboratory of Quantum State Construction and Manipulation (Ministry of Education), Renmin University of China, Beijing 100872, People's Republic of China

<sup>5</sup> Songshan Lake Materials Laboratory, Dongguan, Guangdong 523808, People's Republic of China

E-mail: [hlei@ruc.edu.cn](mailto:hlei@ruc.edu.cn), [ygshi@iphy.ac.cn](mailto:ygshi@iphy.ac.cn), [hxyang@iphy.ac.cn](mailto:hxyang@iphy.ac.cn) and [slli@iphy.ac.cn](mailto:slli@iphy.ac.cn)

Received 23 October 2023, revised 19 December 2023

Accepted for publication 3 January 2024

Published 11 January 2024



## Abstract

The cluster magnet  $\text{Nb}_3\text{Cl}_8$  consists of  $\text{Nb}_3$  trimmers that form an emergent  $S = 1/2$  two-dimensional triangular layers, which are bonded by weak van der Waals interactions. Recent studies show that its room-temperature electronic state can be well described as a single-band Mott insulator. However, the magnetic ground state is non-magnetic due to a structural transition below about 100 K. Here we show that there exists a thickness threshold below which the structural transition will not happen. For a bulk crystal, a small fraction of the sample maintains the high-temperature structure at low temperatures and such remnant gives rise to linear-temperature dependence of the specific heat at very low temperatures. This is further confirmed by the measurements on ground powder sample or *c*-axis pressed single crystals, which prohibits the formation of the non-magnetic state. Moreover, the intrinsic magnetic susceptibility also tends to be constant with decreasing temperature. Our results suggest that  $\text{Nb}_3\text{Cl}_8$  with the high-temperature structure may host a quantum-spin-liquid ground state with spinon Fermi surfaces, which can be achieved by making the thickness of a sample smaller than a certain threshold.

Supplementary material for this article is available [online](#)

Keywords: quantum spin liquids, cluster magnet, specific heat

In searching quantum spin liquids (QSLs), the magnetic moments in frustrated magnets typically sit on individual magnetic ions [1–4]. The idea that clusters of magnetic ions may also give rise to QSLs has attracted increasing interest [5–13]. In these cluster magnets, several magnetic ions form

a cluster and the unpaired electrons are delocalized within it to give a net magnetic moment. The clusters of magnetic ions thus act as spin centers and form emergent frustrated structures. For example, the  $\text{Mo}_3\text{O}_8$ -based cluster magnets have a so-called breathing kagome structure, where the Mo atoms in the small triangles are trimerized with just one  $S = 1/2$  moment and these trimmers form a two-dimensional triangular lattice [14, 15]. Some of these materials, such as  $\text{LiZn}_2\text{Mo}_3\text{O}_8$ ,  $\text{Li}_2\text{ScMo}_3\text{O}_8$ ,  $\text{Li}_2\text{In}_{1-x}\text{Sc}_x\text{Mo}_3\text{O}_8$ , and  $\text{Na}_3\text{Sc}_2\text{Mo}_5\text{O}_{16}$ , show

<sup>6</sup> B Liu, Y Zhang and X Han contributed equally to this work

\* Authors to whom any correspondence should be addressed.

interesting properties that make them good QSL candidates [16–21]. Another example is the  $1T\text{-TaX}_2$  systems ( $X = \text{S}$  or  $\text{Se}$ ), where the spin system formed by 13 Ta molecular clusters may have QSL ground states, as evidenced by recent experiments [22–27] although there are still debates on the role of interlayer couplings [28–35].

The cluster magnet studied in this work is  $\text{Nb}_3\text{Cl}_8$ , which has a trigonal structure at room temperature [36, 37]. Similar to Mo ions in  $\text{Mo}_3\text{O}_8$ -based cluster magnets, the Nb ions have a breathing kagome structure, where three Nb ions form a  $\text{Nb}_3$  trimer that has a  $S = 1/2$  magnetic moment. The trimers thus form an emergent triangular layer and these layers are connected by weak van der Waals' forces without binding cations, which makes the  $\text{Nb}_3\text{X}_8$  ( $X = \text{Cl}, \text{Br}, \text{and I}$ ) systems important for 2D applications [38, 39]. Recent experimental and theoretical studies show that  $\text{Nb}_3\text{Cl}_8$  is a Mott insulator at room temperature that can be well described by the single-band Hubbard model [40–42]. This naturally raises the possibility that the magnetic ground state of  $\text{Nb}_3\text{Cl}_8$  may be a QSL if no magnetic ordering happens. However,  $\text{Nb}_3\text{Cl}_8$  goes through a structural transition below about 100 K and the system becomes nonmagnetic due to interlayer couplings, whose origin is still under debates [36, 37]. This transition thus precludes us from studying the magnetic ground state of the high-temperature magnetic phase (HTMP) in single crystals. Interestingly, it has been found that the HTMP may survive in powder samples obtained by sonicating single crystals [36], which leaves the possibility to investigate the HTMP at low temperatures.

In this paper, we show that the magnetic ground state of HTMP is indeed consistent with the expectation of a QSL with large spinon Fermi surfaces. For single crystals, a small fraction of HTMP survives at low temperatures and its magnetism results in a linear temperature-dependence component of the specific heat, i.e.  $C/T|T \rightarrow 0 = \gamma$ . The HTMP can be further studied by pressing the crystal along  $c$ -axis or grinding single crystals into powders, where the HTMP is maintained in almost the whole sample at low temperatures. The value of  $\gamma$  is found to increase more than one order of magnitude and the intrinsic magnetic susceptibility tends to be constant at low temperatures. Our results suggest that the magnetic ground state of the HTMP of  $\text{Nb}_3\text{Cl}_8$  may be a QSL with large spinon Fermi surfaces.

Single crystals of  $\text{Nb}_3\text{Cl}_8$  and  $\text{Nb}_3\text{Cl}_2\text{Br}_6$  were grown by the flux method as reported previously [36]. Powders were made by grinding single crystals in an agate mortar for just a few minutes. A cold press was used to apply uniaxial pressure along the  $c$ -axis. The structure was studied by a transmission electron microscope (TEM) and a single-crystal x-ray diffractometer. The thickness of the samples in the TEM measurements was determined by the electron energy loss spectroscopy. The specific heat was measured by a physical properties measurement system (Quantum Design, 9 T) with the dilution refrigerator insert. The magnetization was measured by a SQUID magnetometer (Quantum Design, 7 T) with the Helium-3 refrigerator.

Figure 1(a) shows the temperature dependence of the magnetic susceptibility  $\chi = M/H$  for two single crystals, labeled as #1 and #2. As reported previously [36, 37], the high-temperature data can be well fitted by the Curie–Weiss function. The value of  $\chi$  drops dramatically around 100 K with hysteresis behavior between warming and cooling processes, which corresponds to the structural transition accompanied by the magnetic-to-non-magnetic transition [36, 37]. The main difference between these two sets of data is that the remaining value of  $\chi$  in the low-temperature non-magnetic state in #1 sample is smaller than that in sample #2.

The low-temperature magnetism can come from two different sources: the magnetic impurities with orphan spins and the remnant of HTMP [36, 37]. The inset of figure 1(b) shows the field dependence of magnetization at 1.8 K, which can be well fitted by the combination of the Brillouin function with spin  $S = 1/2$  and a linear function, i.e.  $M = NgS\mu_B B(x) + bH$ , where  $N$  is the number of orphan spins,  $g = 2$  is the Landé  $g$ -factor, and  $\mu_B$  is the Bohr magneton. The Brillouin function  $B(x)$  is given by

$$B(x) = \frac{2S+1}{2S} \coth\left(\frac{2S+1}{2J}x\right) - \frac{1}{2J} \coth\left(\frac{1}{2J}x\right), \quad (1)$$

where  $x = g\mu_B SB/k_B T$ . The value of  $N$  is about 0.88% per molecular formula for both samples. On the other hand, the slope of the linear function, denoted as  $b$ , is about  $4.3 \times 10^{-4}$  and  $1.6 \times 10^{-3} \text{ emu mol}^{-1} \text{ Oe}$  for #1 and #2 samples, respectively. The larger value of  $b$  in #2 sample indicates that it has a larger fraction of HTMP at low temperatures.

Figure 1(c) shows the low-temperature specific heat of #1 sample at different magnetic fields. A broad peak appears at about 0.4 K at 1 T and shifts to higher temperature with increasing field. Figure 1(d) shows the difference between the specific heat under field  $B$  and that at zero field, i.e.  $\Delta C = C(B) - C(0)$ . We find that it can be well fitted by the Schottky anomaly function  $C_{\text{SA}}$  with  $\Delta C = C_{\text{SA}}(B) - C_{\text{SA}}(0)$ . Here  $C_{\text{SA}}(B) = NR(\Delta/T)^2 \exp(\Delta/T) / [1 + \exp(\Delta/T)]^2$  with  $\Delta = [\Delta_0^2 + (gS\mu_B B)^2]^{1/2}$ , where  $N$ ,  $R$ ,  $g$ ,  $\Delta_0$  and  $\mu_B$  are the number of spins per molecular formula, the gas constant, the  $g$ -factor, the internal energy level at zero field, and Bohr magneton, respectively. The fittings give the value of  $N$  between 0.86% to 0.89%, which are very close to the number of orphan spins determined from the magnetization data. This means that the field dependence of the specific heat mainly comes from the orphan spins and we can thus derive the intrinsic specific heat  $C_{\text{inc}}$  by subtracting  $C_{\text{SA}}$  from the data, as shown in figure 1(e). A similar analysis procedure can also be applied to the specific heat of #2 sample, as shown in figure 1(f).

For both samples, there are sharp upturns when the temperature goes to zero, which come from the contribution of nuclear Schottky anomaly [43]. It seems that a finite intercept at 0 K is present in  $C/T$  for both samples. The zero-K extrapolation of  $C/T$  gives the value of the linear term  $\gamma$  as about 0.016 and 0.08  $\text{J mol K}^{-2}$  for #1 and #2 samples, respectively. The ratio between these two  $\gamma$  is similar to that between the value

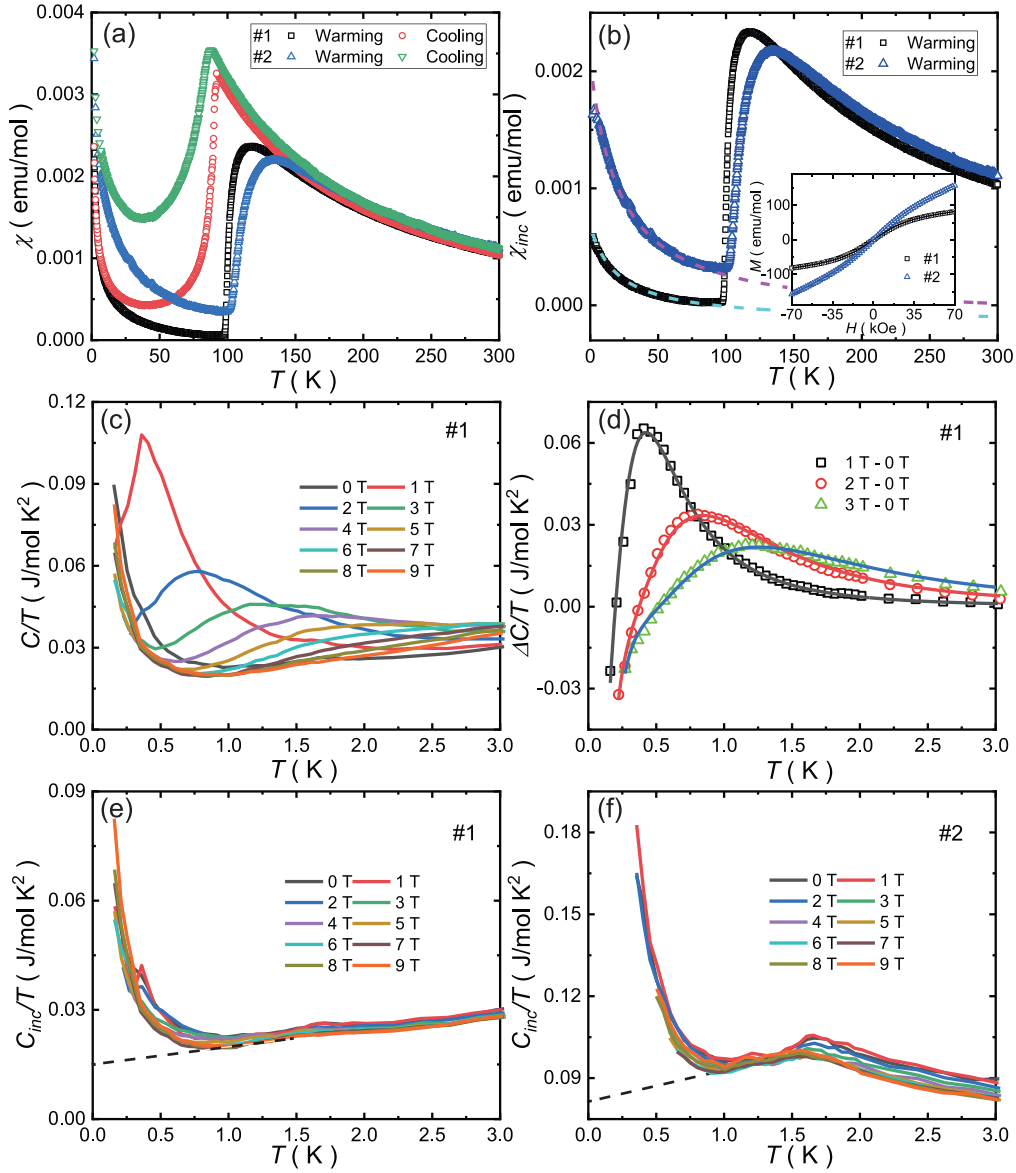


**Figure 1.** (a) The temperature dependence of magnetic susceptibility  $\chi = M/H$  at 0.1 T for #1 and #2 single crystals. (b) The intrinsic magnetic susceptibility in the warming process for #1 and #2 single crystals after subtracting the impurity contribution. The dashed lines are results of the high-temperature Curie-Weiss fittings multiplied by 0.045 and 0.11 for #1 and #2 samples, respectively. The fitted Weiss temperatures and effective moment for #1 single crystal are  $-21.5$  K and  $1.762 \mu_B$ , respectively, while those for #2 single crystal are  $-18.1$  K and  $1.771 \mu_B$ . The inset shows the field dependence of magnetization at 1.8 K. The solid lines are fitted by the Brillouin function plus a linear background. (c) The  $C/T$  of #1 single crystal as the function of temperature. (d) The temperature dependence of  $\Delta C/T$  with  $\Delta C = C(B) - C(0)$  at  $B = 1, 2,$  and  $3$  T. The solid lines are fitted results of the field difference between the Schottky anomaly function as described in the main text. (e) and (f) The intrinsic specific heat  $C_{inc}/T$  after subtracting the contribution from the Schottky anomaly. The dashed lines are guides to the eye.

of  $b$  in  $M-H$  curves, suggesting both  $\gamma$  and  $b$  come from the remnant of the HTMP.

While the above results suggest the existence of the HTMP, its exact properties are rather hard to study due to its small fractions in single-crystal samples. We note that #2 single crystal was accidentally pressed in the capsule during the magnetic measurements, which may result in a larger fraction of the HTMP. Therefore, we intentionally pressed #3 single crystal at about 1.8 GPa along the  $c$ -axis. The single-crystal x-ray

diffraction measurement shows that the room-temperature crystal structure remains the same but there are many small grains present within the sample [43]. Figure 2(a) shows the temperature dependence of magnetic susceptibility, which suggests that more than 80% HTMP survive at low temperatures. The fitting on the field dependence of magnetization at 1.8 K (figure 2(c)) suggests the existence of 0.3% orphan spins. The slope of  $M-H$  curve,  $b$ , is  $9.77 \times 10^{-3} \text{ emu mol}^{-1} \text{ Oe}$ , much larger than those of #1 and #2 single crystals. The

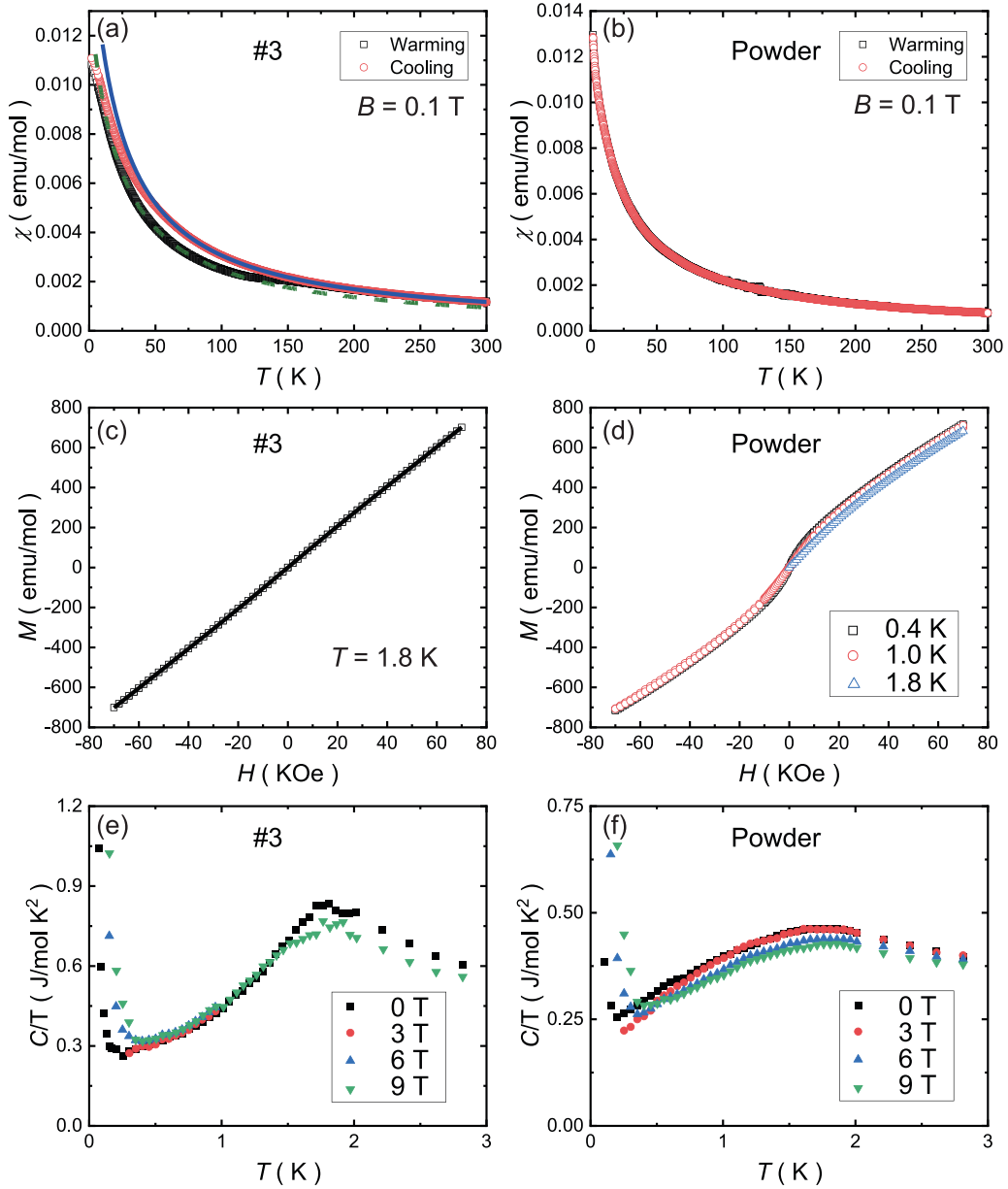


**Figure 2.** (a) and (b) The temperature dependence of magnetic susceptibility  $\chi$  at 1000 Oe for #3 single crystal and ground powders, respectively. The solid line in (a) is the fitted result by the Curie–Weiss function for the cooling data. The dotted line in (a) is the result of the Curie–Weiss fitting multiplied by 0.8. The fitted Weiss temperature and effective moment for #3 single crystal are  $-20$  K and  $1.76 \mu_B$ , respectively, while those for powders are  $-15.8$  K and  $1.47 \mu_B$ . (c) and (d) Field dependence of magnetization at low temperatures for #3 single crystal and ground powders, respectively. The solid lines are fitted by the Brillouin function plus a linear background. (e) and (f) Low-temperature specific heats of #3 single crystal and ground powders, respectively.

low-temperature specific heats are given in figure 2(e) and show little field dependence. The zero-K extrapolation of  $C/T$  gives  $\gamma \approx 0.223$  J mol  $K^{-2}$  at 0 T.

As shown in [36], the HTMP can also be maintained in ground powders. The temperature dependence of the susceptibility of our powder sample is shown in figure 2(b), which confirms the absence of magnetic transition or crossover. The  $M-H$  curves (figure 2(d)) give the content of orphan spins as about 2.5%, most of which may come from the surfaces of small grains [44]. The slope of  $M-H$  curve at high fields at 1.8 K is similar to that in the #3 sample and changes little with

temperature decreasing down to 0.4 K. This suggests that the magnetic susceptibility tends to a constant when approaching zero K. The low-temperature specific heat also shows weak field dependence and  $\gamma$  is about  $0.227$  J mol  $K^{-2}$  at 0 T, as shown in figure 2(f).

To understand why there is a remnant of the HTMP even in a single-crystal sample, we studied the low-temperature structure by TEM. However, the structural transition in  $Nb_3Cl_8$  is below 100 K, which makes it hard to study its structure using TEM. As the transition temperature can be increased continuously by partial replacement of Cl by Br [45], we

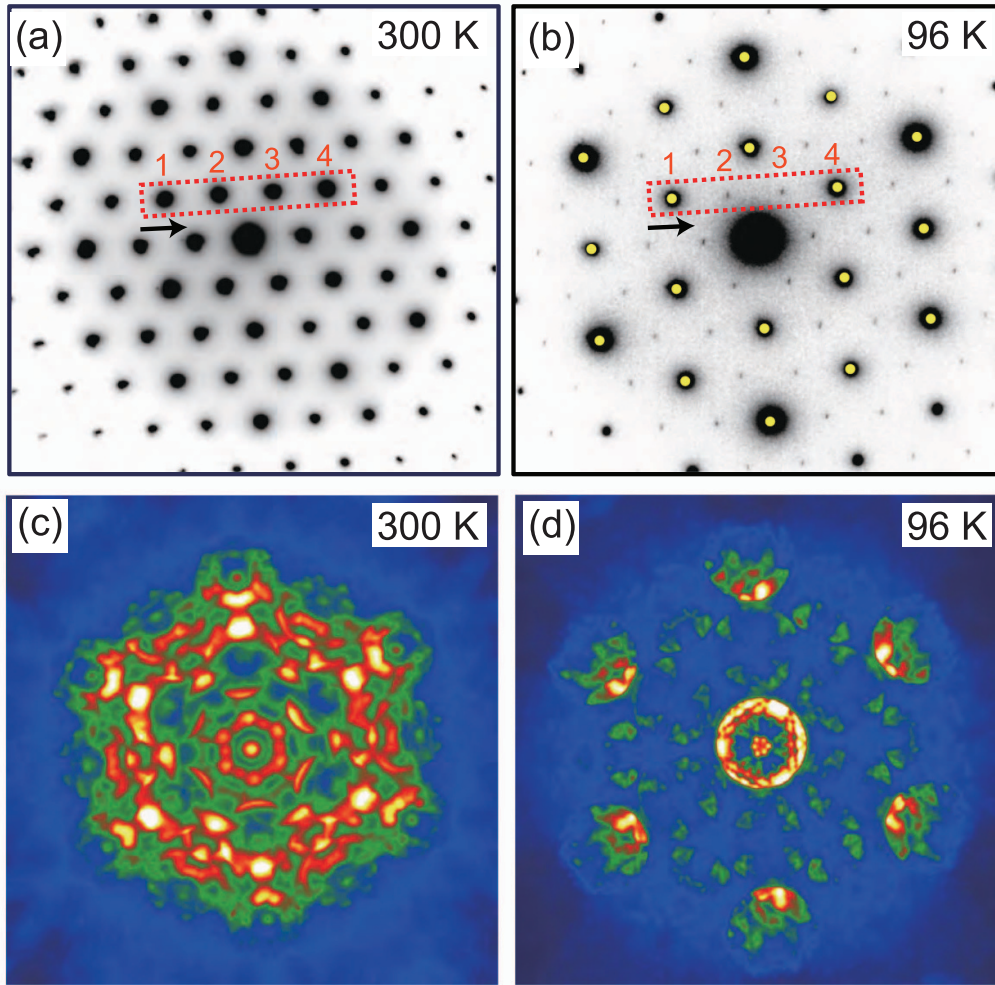


**Figure 3.** (a) and (b) SAED results of  $\text{Nb}_3\text{Cl}_2\text{Br}_6$  with the electron beam along the  $c$ -axis at 300 and 96 K, respectively. The dotted rectangles label the four peaks whose intensities cut along the arrows are shown in figure 4(a). The peaks labeled 1, 2, 3 and 4 correspond to  $(2, -1, 0)$ ,  $(1, 0, 0)$ ,  $(0, 1, 0)$  and  $(-1, 2, 0)$  in the trigonal notation. The yellow dots in (b) represent the positions of the Bragg peaks in the  $R3$  structure. (c) and (d) CBED results of  $\text{Nb}_3\text{Cl}_2\text{Br}_6$  with the beam along the  $c$ -axis at 300 and 96 K, respectively.

choose to study the structure of  $\text{Nb}_3\text{Cl}_2\text{Br}_6$  whose structural transition occurs slightly below 300 K. Figure 3(a) shows the results of selected area electron diffraction (SAED) at 300 K with the electron beam along the  $c$ -axis. All the peaks can be indexed by the trigonal structure with the space group  $P\bar{3}m1$  as reported previously [36, 37]. At 96 K which is well below the structural transition temperature, the major peaks can be indexed by the  $R3$  space group as shown in figure 3(b). There are two reported low-temperature structures, namely  $R3$  and  $C2/m$  [36, 37], which can be distinguished by the three-fold  $C_3$  rotational symmetry. As shown by the patterns around the centers in the convergent beam electron diffraction (CBED) images (figures 3(c) and (d)), the in-plane rotational symmetry changes from  $C_6$  at 300 K to  $C_3$  at 96 K, which is consistent with the  $R3$  structure and thus rules out the  $C2/m$  structure.

We note that there are weak peaks in figure 3(b) that correspond to the  $P\bar{3}m1$  structure, which suggests that a small fraction of the samples maintains its high-temperature structure as

shown previously [36, 37]. We further measure a single-crystal sample at two different regions labeled as A and B, as shown in the inset of figure 4(a). Region B is at the edge of the sample and has a smaller thickness. Figure 4(a) shows the cut along the four Bragg peaks as indicated in figures 3(a) and (b). The residual peak intensities at  $(1, 0, 0)$  and  $(0, 1, 0)$  at 96 K are very different for regions A and B, which suggests that the remnant of the high-temperature structure is greater in thinner part of the sample. The thickness dependence of the structural transition can be quantitatively studied by the intensity ratio between 98 and 300 K for the  $(1, 0, 0)$  peak. An abrupt change happens around 10 nm as shown in figure 4(b), below which the ratio is close to 1, suggesting that no structural transition happens. We note this thickness threshold is close to three times of the  $c$ -axis in the low-temperature structure of the bulk sample, which indicates that at least three unit cells along the  $c$ -axis are needed to form the  $R3$  structure. This may explain why a moderate uniaxial pressure can significantly increase the proportion of HTMP at low temperatures since it may weaken or

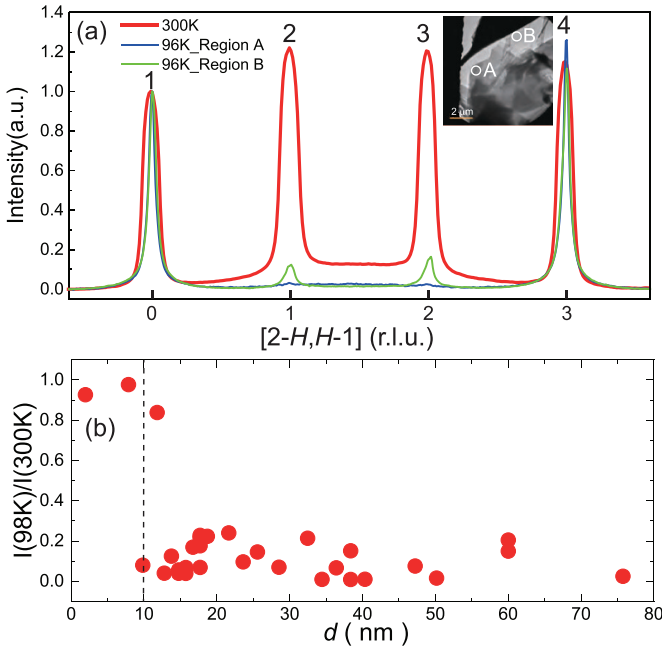


**Figure 4.** (a) Normalized intensities cut along the arrows in (a) and (b). The measured regions of A and B are shown by the circles on the sample in the inset. (b) Thickness dependence of the ratio of peak intensity at (1,0,0) between 98 and 300 K.

destroy the interlayer couplings and thus prevent the formation of the  $R3$  structure.

The above results show a prominent property of the HTMP in  $Nb_3Cl_8$ , i.e. a large linear- $T$  term in the specific heat when the temperature goes to zero. The  $\gamma$  values in #3 and powder sample are much larger than those of typical metals. As there is no magnetic transition, such linear- $T$  term of the specific heat may be attributed to spinon Fermi surfaces in a QSL [1–4]. Moreover, the magnetic susceptibility also seems to be a constant below 1.8 K as shown in figure 2(d), which is also consistent with the existence of spinon Fermi surfaces. An interesting parameter that may describe the spinon system is the Wilson ratio [1, 46], which is defined as

$$R_w = \frac{4\pi^2 k_B^2 \chi}{3\mu_0 (g\mu_B)^2 \gamma}, \quad (2)$$

where  $k_B$ ,  $\mu_0$  and  $\mu_B$  are Boltzmann constant, vacuum magnetic permeability, and Bohr magneton, respectively. The value of  $R_w$  is 1 for a free electron gas. In our case,  $R_w$  is about 1.8, 1.4, 2.6 and 2.9 for #1, #2 and #3 single crystals and powder sample, respectively. All these values are close to 1, further suggesting the existence of spinon Fermi surfaces.

While the above results are intriguing, an important unresolved issue is whether the magnetic properties obtained in pressed single crystal or powder are the true ground state of  $Nb_3Cl_8$  if no structural transition happens. We note that the slope of  $M - H$  curve and  $\gamma$  do not depend linearly on the fraction of HTMP determined from the temperature dependence of the susceptibility. The specific heat also shows some sample-dependent behaviors at low temperatures. For example, the

hump at about 1.8 K is much broader in powder sample (figure 2(f)) than the #3 sample (figure 2(c)). One optimistic explanation is that the physical properties associated with the spinon Fermi surfaces have in-plane size dependence, as in metal particles [47] or some of the QSLs [44]. However, although the main structure remains the same [43], we cannot rule out the possibility that the structure might be deformed or distort locally, which may in turn alter the magnetic properties. We would like to emphasize though that a large zero-K  $C/T$  always exists despite detailed differences in the specific heat. Since the layers in  $Nb_3Cl_8$  are connected by van der Waals interactions, the nature of the magnetic ground state may be further studied in nanosheets where the HTMP is expected to survive at 0 K.

In conclusion, we show that the magnetic phase in  $Nb_3Cl_8$  can partially survive at low temperatures in single crystals or powder samples. Moreover, the low-temperature specific-heat and magnetization measurements suggest that it may have spinon Fermi surfaces. This is consistent with the suggestion that  $Nb_3Cl_8$  is a Mott insulator [40]. Further local measurements, such as inelastic neutron scattering and nuclear magnetic resonance, may provide more insights into the nature of the magnetic ground state for the high-temperature structure of  $Nb_3Cl_8$ .

### Data availability statement

All data that support the findings of this study are included within the article (and any supplementary files).

### Acknowledgments

We thank Prof. Tian Qian and Prof. Yi Zhou for helpful discussions. This work is supported by the National Key Research and Development Program of China (Grant Nos. 2021YFA1400401, 2022YFA1403400, 2018YFE0202600 and 2022YFA1403800), the National Natural Science Foundation of China (Nos. U2032204 and 11774423), the Chinese Academy of Sciences (Grant Nos. XDB33000000, XDB33010000, CAS-WX2021SF-0102, and GJTD-2020-01), and the Synergetic Extreme Condition User Facility (SECUF).

### ORCID iDs

Jianping Sun <https://orcid.org/0000-0002-2873-6023>  
 Jinguang Cheng <https://orcid.org/0000-0002-4969-1960>  
 Hechang Lei <https://orcid.org/0000-0003-0850-8514>  
 Shiliang Li <https://orcid.org/0000-0001-7922-3730>

### References

- [1] Balents L 2010 Spin liquids in frustrated magnets *Nature* **464** 199
- [2] Savary L and Balents L 2017 Quantum spin liquids: a review *Rep. Prog. Phys.* **80** 016502

- [3] Zhou Y, Kanoda K and Ng T-K 2017 Quantum spin liquid states *Rev. Mod. Phys.* **89** 025003
- [4] Broholm C, Cava R J, Kivelson S A, Nocera D G, Norman M R and Senthil T 2020 Quantum spin liquids *Science* **367** 263
- [5] Chamorro J R, McQueen T M and Tran T T 2021 Chemistry of quantum spin liquids *Chem. Rev.* **121** 2898
- [6] Chen G, Kee H-Y and Baek Kim Y 2016 Cluster Mott insulators and two Curie-Weiss regimes on an anisotropic kagome lattice *Phys. Rev. B* **93** 245134
- [7] Chen G and Lee P A 2018 Emergent orbitals in the cluster Mott insulator on a breathing kagome lattice *Phys. Rev. B* **97** 035124
- [8] Schaffer R, Huh Y, Hwang K and Kim Y B 2017 Quantum spin liquid in a breathing kagome lattice *Phys. Rev. B* **95** 054410
- [9] Yao X-P, Zhang X-T, Kim Y B, Wang X and Chen G 2020 Clusterization transition between cluster Mott insulators on a breathing kagome lattice *Phys. Rev. Res.* **2** 043424
- [10] Nikolaev S A, Solovyev I V and Streltsov S V 2021 Quantum spin liquid and cluster Mott insulator phases in the  $\text{Mo}_3\text{O}_8$  magnets *npj Quantum Mater.* **6** 25
- [11] Law K T and Lee P A 2017 1T-TaS<sub>2</sub> as a quantum spin liquid *Proc. Natl Acad. Sci. USA* **114** 6996
- [12] He W-Y, Xu X Y, Chen G, Law K T and Lee P A 2018 Spinon fermi surface in a cluster Mott insulator model on a triangular lattice and possible application to 1T-TaS<sub>2</sub> *Phys. Rev. Lett.* **121** 046401
- [13] Li C-K, Yao X-P, Liu J and Chen G 2022 Fractionalization on the surface: is type-II terminated 1T-TaS<sub>2</sub> surface an anomalously realized spin liquid? *Phys. Rev. Lett.* **129** 017202
- [14] Torardi C C and McCarley R E 1985 Synthesis, crystal structures and properties of  $\text{LiZn}_2\text{Mo}_3\text{O}_8$ ,  $\text{Zn}_3\text{Mo}_3\text{O}_8$  and  $\text{ScZnMo}_3\text{O}_8$ , reduced derivatives containing the  $\text{Mo}_3\text{O}_{13}$  cluster unit *Inorg. Chem.* **24** 476
- [15] Sheckelton J P, Neilson J R, Soltan D G and McQueen T M 2012 Possible valence-bond condensation in the frustrated cluster magnet  $\text{LiZn}_2\text{Mo}_3\text{O}_8$  *Nat. Mater.* **11** 493
- [16] Sheckelton J P et al 2014 Local magnetism and spin correlations in the geometrically frustrated cluster magnet  $\text{LiZn}_2\text{Mo}_3\text{O}_8$  *Phys. Rev. B* **89** 064407
- [17] Mourigal M, Fuhrman W T, Sheckelton J P, Wartelle A, Rodriguez-Rivera J A, Abernathy D L, McQueen T M and Broholm C L 2014 Molecular quantum magnetism in  $\text{LiZn}_2\text{Mo}_3\text{O}_8$  *Phys. Rev. Lett.* **112** 027202
- [18] Haraguchi Y, Michioka C, Imai M, Ueda H and Yoshimura K 2015 Spin-liquid behavior in the spin-frustrated  $\text{Mo}_3$  cluster magnet  $\text{Li}_2\text{ScMo}_3\text{O}_8$  in contrast to magnetic ordering in isomorphous  $\text{Li}_2\text{InMo}_3\text{O}_8$  *Phys. Rev. B* **92** 014409
- [19] Akbari-Sharbat, Sinclair R, Verrier A, Ziat D, Zhou H D, Sun X F and Quilliam J A 2018 Tunable quantum spin liquidity in the 1/6th-filled breathing kagome lattice *Phys. Rev. Lett.* **120** 227201
- [20] Iida K et al 2019 Quantum magnetisms in uniform triangular lattices  $\text{Li}_2\text{AMo}_3\text{O}_8$  (A = In, Sc) *Sci. Rep.* **9** 1826
- [21] Chen Q et al 2022 Magnetic order and spin liquid behavior in  $[\text{Mo}_3]^{1+}$  molecular magnets *Phys. Rev. Mater.* **6** 044414
- [22] Kratochvilova M, Hillier A D, Wildes A R, Wang L, Cheong S-W and Park J-G 2017 The low-temperature highly correlated quantum phase in the charge-density-wave 1T-TaS<sub>2</sub> compound *npj Quantum Mater.* **2** 42
- [23] Klanjšek M, Zorko A, Žitko R, Mravlje J, Jagličić Z, Biswas P K, Prelovšek P, Mihailović D and Arčon D 2017 A high-temperature quantum spin liquid with polaron spins *Nat. Phys.* **13** 1130
- [24] Ribak A, Silber I, Baines C, Chashka K, Salman Z, Dagan Y and Kanigel A 2017 Gapless excitations in the ground state of 1T-TaS<sub>2</sub> *Phys. Rev. B* **96** 195131
- [25] Chen Y et al 2020 Strong correlations and orbital texture in single-layer 1T-TaS<sub>2</sub> *Nat. Phys.* **16** 218
- [26] Ruan W et al 2021 Evidence for quantum spin liquid behaviour in single-layer 1T-TaS<sub>2</sub> from scanning tunnelling microscopy *Nat. Phys.* **17** 1154
- [27] Mañas-Valero S, Huddart B M, Lancaster T, Coronado E and Pratt F L 2021 Quantum phases and spin liquid properties of 1T-TaS<sub>2</sub> *npj Quantum Mater.* **6** 69
- [28] Ritschel T, Berger H and Geck J 2018 Stacking-driven gap formation in layered 1T-TaS<sub>2</sub> *Phys. Rev. B* **98** 195134
- [29] Lee S-H, Goh J S and Cho D 2019 Origin of the insulating phase and first-order metal-insulator transition in 1T-TaS<sub>2</sub> *Phys. Rev. Lett.* **122** 106404
- [30] Martino E et al 2020 Preferential out-of-plane conduction and quasi-one-dimensional electronic states in layered 1T-TaS<sub>2</sub> *npj 2D Mater. Appl.* **4** 7
- [31] Butler C J, Yoshida M, Hanaguri T and Iwasa Y 2020 Mottness versus unit-cell doubling as the driver of the insulating state in 1T-TaS<sub>2</sub> *Nat. Commun.* **11** 2477
- [32] Lee J, Jin K-H and Yeom H W 2021 Distinguishing a Mott insulator from a trivial insulator with atomic adsorbates *Phys. Rev. Lett.* **126** 196405
- [33] Shin D, Tancogne-Dejean N, Zhang J, Okyay M S, Rubio A and Park N 2021 Identification of the Mott insulating charge density wave state in 1T-TaS<sub>2</sub> *Phys. Rev. Lett.* **126** 196406
- [34] Petocchi F, Nicholson C W, Salzmann B, Pasquier D, Yazyev O V, Monney C and Werner P 2022 Mott versus hybridization gap in the low-temperature phase of 1T-TaS<sub>2</sub> *Phys. Rev. Lett.* **129** 016402
- [35] Wu Z, Bu K, Zhang W, Fei Y, Zheng Y, Gao J, Luo X, Liu Z, Sun Y-P and Yin Y 2022 Effect of stacking order on the electronic state of 1T-TaS<sub>2</sub> *Phys. Rev. B* **105** 035109
- [36] Haraguchi Y, Michioka C, Ishikawa M, Nakano Y, Yamochi H, Ueda H and Yoshimura K 2017 Magnetic-nonmagnetic phase transition with interlayer charge disproportionation of Nb<sub>3</sub> trimers in the cluster compound Nb<sub>3</sub>Cl<sub>8</sub> *Inorg. Chem.* **56** 3483
- [37] Sheckelton J P, Plumb K W, Trump B A, Broholm C L and McQueen T M 2017 Rearrangement of van der Waals stacking and formation of a singlet state at  $T = 90$  K in a cluster magnet *Inorg. Chem. Front.* **4** 481
- [38] Wang M-C et al 2020 Prospects and opportunities of 2d van der Waals magnetic systems *Ann. Phys.* **532** 1900452
- [39] Wu H, Wang Y, Xu Y, Sivakumar P K, Pasco C, Filippozzi U, Parkin S S P, Zeng Y-J, McQueen T and Ali M N 2022 The field-free Josephson diode in a van der Waals heterostructure *Nature* **604** 653
- [40] Gao S et al 2023 Discovery of a single-band Mott insulator in a van der Waals flat-band compound *Phys. Rev. X* **13** 041049
- [41] Zhang Y, Gu Y, Weng H, Jiang K and Hu J 2023 Mottness in two-dimensional van der Waals Nb<sub>3</sub>X<sub>8</sub> monolayers (X = Cl, Br, and I) *Phys. Rev. B* **107** 035126
- [42] Grytsiuk S, Katsnelson M I, van Loon E G C P and Rösner M 2023 Nb<sub>3</sub>Cl<sub>8</sub>: a prototypical layered Mott-Hubbard insulator (arXiv:2305.04854)
- [43] See supplemental material
- [44] Wei Y et al 2021 Nonlocal effects of low-energy excitations in quantum-spin-liquid candidate Cu<sub>3</sub>Zn(OH)<sub>6</sub>FBr *Chin. Phys. Lett.* **38** 097501
- [45] Pasco C M, Baggari I E, Bianco E, Kourkoutis L F and McQueen T M 2019 Tunable magnetic transition to a singlet ground state in a 2D van der Waals layered trimerized kagome magnet *ACS Nano* **13** 9457
- [46] Prelovšek P, Morita K, Tohyama T and Herbrich J 2020 Vanishing Wilson ratio as the hallmark of quantum spin-liquid models *Phys. Rev. Res.* **2** 023024
- [47] Halperin W P 1986 Quantum size effects in metal particles *Rev. Mod. Phys.* **58** 533–606